11th World Congress on Computational Mechanics (WCCM XI)
5th European Conference on Computational Mechanics (ECCM V)
6th European Conference on Computational Fluid Dynamics (ECFD VI)
E. Oñate, J. Oliver and A. Huerta (Eds)

ON THE INTEGRATION OF HIGH-ORDER BOUNDARY ELEMENTS IN A 3D DISCONTINUOUS GALERKIN METHOD FOR TURBOMACHINERY FLOWS

Svetlana Drapkina*, Christian Frey, and Graham Ashcroft

German Aerospace Center (DLR)
Institute of Propulsion Technology
Linder Höhe, 51147 Cologne, Germany
e-mail: {svetlana.drapkina, christian.frey, graham.ashcroft@dlr.de}

Key words: Curved Boundary Elements, High-Order Discontinuous Galerkin

Abstract. This paper describes the integration of a Discontinuous Galerkin (DG) solver into the DLR flow solver TRACE which solves the three-dimensional compressible Navier-Stokes equations on structured and unstructured grids. Special emphasis is put on the integration of the DG approach into the process chain for turbomachinery applications which requires extension for the generation of curved boundary elements and the visualization of high-order elements.

1 INTRODUCTION

Global air traffic is forecast to grow significantly in the coming years. To facilitate this development, particularly in the context of ambitious environmental goals concerning the reduction of emissions and noise pollution, there is a great need for new and more efficient engine technologies. To accurately investigate such technologies, and at the same time realize the shorter development cycles demanded by customers, more efficient, flexible and accurate numerical tools for the simulation of turbomachinery flows are essential.

In this context, high-order accurate numerical methods suitable for application on unstructured grids represent an attractive solution. One of the most popular high-order methods for unstructured grids is the Discontinuous Galerkin (DG) finite element method. The DG method may be considered as a combination of the Finite Volume (FV) and Finite Element (FE) methods in which the solution is approximated by means of piecewise polynomials inside the elements and, in contrast to standard FE methods, continuity between adjacent elements is not required.

The DG method was first introduced in [9] for the neutron transport equation. Cockburn and Shu extended the spatial DG discretization to hyperbolic non-linear conservation laws. An explicit high-order Runge-Kutta time discretization in combination with DG is

presented in [5, 6]. An overview of convection-dominated problems concerning theoretical and computational aspects of DG methods appears in [3, 4]. Progress of high-order DG methods in the context of aerospace applications is discussed in [8].

The importance of accurate approximation of geometric boundaries for DG has been pointed out by many authors, cf. [1, 7, 8]. It is shown that solution accuracy degrades near the boundaries if straight edges are used. Moreover, the local refinement of the mesh does not improve the accuracy near the boundaries.

Therefore, in this work for cells adjacent to curved solid wall boundaries the standard linear parametrization is replaced with a polynomial representation ($q > 1$). The transformation from a reference element to the curved element is expressed in terms of Lagrange polynomials and is calculated from additional points on the curved boundary. The corresponding formulas for the Jacobians of 2D and 3D elements and the face normal vectors are adapted.

The three-dimensional DG solver presented here, represents the further development of the two-dimensional DG solver demonstrated in [2]. Although the DG solver employs up to fourth order elements for the spatial discretization, the generation of appropriate meshes with high-order elements and the visualization of solutions on these elements is not provided by commercial tools. Therefore, the pre- and post-processing [10] tools of the TRACE process chain, have been extended.

The paper is organized as follows. In Section 2 the governing equations are presented. Furthermore, the DG method for the spatial discretization and the time discretization scheme are introduced. The treatment of curved boundaries is described in Section 3. The process chain for turbomachinery applications with high-order elements, the generation of curved boundaries and their application to a numerical test case are presented in Sections 4 and 5, respectively. The results are summarized in Section 6.

2 DISCRETIZATION

DLR's in-house CFD code TRACE is a second-order FV solver for the Reynolds-averaged Navier-Stokes equations. It has been developed at DLR's Institute of Propulsion Technology. The aim of the integration of the high-order DG spatial discretization into the TRACE framework is to provide an efficient tool for turbomachinery simulation problems where highly accurate solutions are required. In this work, we describe in detail the DG discretization method for the Euler equations.

2.1 Governing Equations

Three-dimensional compressible inviscid flow is described by the Euler equations. We solve the Euler equations in conservative form i.e.,

$$\frac{\partial q}{\partial t} + \nabla \cdot F(q) = 0 \qquad \text{in } \Omega \times (0, T) \tag{1}$$

with some initial and boundary conditions. $T > 0$ represents the final time and $\Omega \subset \mathbb{R}^3$ is a bounded domain. The Cartesian components of the conservative state vector q and flux vectors $\langle F(q), \vec{n}\rangle = F^{\vec{n}}(q)$ are

$$q = \begin{pmatrix} \rho \\ \rho U \\ \rho E \end{pmatrix}, \qquad F^{\vec{n}}(q) = \begin{pmatrix} \rho\langle U, \vec{n}\rangle \\ \rho\langle U, \vec{n}\rangle + p\vec{n} \\ \rho\langle U, \vec{n}\rangle H \end{pmatrix},$$

where $\vec{n} = (n_x, n_y, n_z)$ is the outward unit normal to the boundary, ρ is the density, E is the total energy and $U = (u, v, w)$ are the velocity components in the x, y and z directions, respectively. H is the total enthalpy per unit mass and is defined as $H = \frac{\gamma}{(\gamma-1)}\frac{p}{\rho} + \frac{1}{2}\|U\|^2$, where $\gamma = 1.4$ is the ratio of specific heats and p is the pressure. The pressure is related to the other thermodynamic variables by the equation of state for an ideal gas, such that $p = (\gamma - 1)\rho[E - \frac{1}{2}\|U\|^2]$.

2.2 The Discontinuous Galerkin Scheme

In this section in order to provide the necessary notations the DG discretization method is summarized. The weak formulation of equation (1) follows in a standard way, cf. [4].

Suppose, the domain Ω is a collection of arbitrary non-overlapping elements Ω_i, such that $\Omega = \cup_{i=1,\ldots,N_{\text{el}}}\Omega_i$, where N_{el} denotes the number of 3D elements in the domain. First of all, the construction of a discrete space will be outlined. The DG discretization uses polynomial bases which are discontinuous across the elements. Therefore, the space of piece-wise polynomials is defined as,

$$V_h = \{v_h \in L^2(\Omega) \;\big|\; v_{h|_{\Omega_i}} \in \mathcal{P}^p(\Omega_i) \quad \text{for all } i = 1, \ldots, N_{\text{el}}\},$$

where $\mathcal{P}^p(\Omega_i)$ denotes the set of polynomials of degree up to p defined on the cell Ω_i and h stands for a discretization parameter.

The weak formulation is obtained by multiplying equation (1) by a sufficiently smooth test function v and performing integration by parts

$$\int_{\Omega_i} v\frac{\partial q(x,t)}{\partial t}\, d\Omega_i + \oint_{\partial\Omega_i} vF^{\vec{n}}(q(x,t))\, dA - \int_{\Omega_i} F^{\nabla_x v}(q(x,t))\, d\Omega_i = 0. \tag{2}$$

Further, in order to find an approximation of $q(x,t)$ such that, for each time $t \in [0,T]$, the discrete function $q_h(x,t)$ belongs to V_h, where $x = (x_1, x_2, x_3)$, we substitute $q(x,t)$ and v by their polynomial expansions.

Let $\phi_1(x), \ldots, \phi_{n(p)}(x)$ be a basis of $\mathcal{P}^p(\Omega_i)$. Therefore, a function $v_h \in \mathcal{P}^p(\Omega_i)$ has the representation

$$v_{h,i}(x) = \sum_{k=1}^{n(p)} v_{i,k}\phi_{i,k}(x),$$

i.e., each test function $v_h \in \mathcal{P}^p(\Omega_i)$ can be written as a linear combination of the basis functions $\phi_{i,k}(x)$. The number of degrees of freedom for the polynomial basis of the order p in every element is denoted by $n(p)$. Since $q_h(x,t)$ belongs to the same subspace V_h with the basis $\phi_1(x), \ldots, \phi_{n(p)}(x)$, it satisfies the following

$$q_{h,i}(x,t) = \sum_{l=1}^{n(p)} q_{i,l}(t)\phi_{i,l}(x). \tag{3}$$

Now the basic discrete form of the DG approach can be described

$$\int_{\Omega_i} v_h \frac{\partial q_h(x,t)}{\partial t}\, d\Omega_i + \sum_{\sigma=\sigma_{i,j}\in\partial\Omega_i} \oint_\sigma v_h F^{\vec{n}_\sigma}_{\text{num}}(q_{h,i}(x,t), q_{h,j}(x,t))\, dA - \int_{\Omega_i} F^{\nabla_x v_h}(q_h(x,t))\, d\Omega_i = 0. \tag{4}$$

The flux $F^{\vec{n}_\sigma}(q(x,t))$ in (2) is replaced by a numerical flux function $F^{\vec{n}_\sigma}_{\text{num}}(q_{h,i}(x,t), q_{h,j}(x,t))$, which depends on the outward unit vector w. r. t. the face $\vec{n}_\sigma$, local interface state $q_{h,i}$ and the interface state $q_{h,j}$ of the neighbouring element. For the current DG code the Roe numerical flux is employed. The set of faces of the element Ω_i in (4) are denoted by $\partial\Omega_i$. $\sigma_{i,j}$ is the face between the elements i and j.

Replacing $q_h(x,t)$ in (4) by (3) and testing (4) only against the basis functions $\phi_{i,k}(x)$ for all $k = 1, \ldots, n(p)$, yields

$$\frac{\partial q_{i,l}(t)}{\partial t} \int_{\Omega_i} \phi_{i,k}(x)\phi_{i,l}(x)\, d\Omega_i + \sum_{\sigma=\sigma_{i,j}\in\partial\Omega_i} \oint_\sigma \phi_{i,k}(x) F^{\vec{n}_\sigma}_{\text{num}}(q_{h,i}(x,t), q_{h,j}(x,t))\, dA - \int_{\Omega_i} F^{\nabla_x \phi_{i,k}}(q_{h,i}(x,t))\, d\Omega_i = 0. \tag{5}$$

Substituting integrals of the mass matrix, numerical flux and the stiffness term by M, H and S, respectively, equation (5) can be rewritten in the compact form

$$\frac{\partial q_{i,l}(t)}{\partial t} + R^i_l = 0$$

with $R^i_l = \tilde{M}^i_{lk}\big(H^i_k - S^i_k\big)$ and $\tilde{M}^i_{lk} M^i_{kl} = I$. The volume integrals in M^i_{kl} and S^i_k and the surface integrals H^i_k are carried out using numerical Gauss quadrature formulas of appropriate order of accuracy, cf. [3], in the following form

$$H^i_k = \sum_{\sigma=\sigma_{i,j}\in\partial\Omega_i} \sum_{x\in\mathcal{G}_\sigma} \omega_{\sigma,x}\phi_{i,k}(x) F^{\vec{n}_\sigma}_{\text{num}}(q_{h,i}(x), q_{h,j}(x))|\sigma| \tag{6}$$

$$S^i_k = \sum_{x\in\mathcal{G}_{\Omega_i}} \omega_{\Omega_i,x} F^{\nabla_x \phi_{i,k}(x)}(q_{h,i}(x))|\Omega_i|, \tag{7}$$

where the set of two-dimensional Gauss integration points is denoted by $\mathcal{G}_\sigma$ and the set of three-dimensional Gauss integration points is denoted by $\mathcal{G}_{\Omega_i}$. The two- and three-dimensional integration weights are $\omega_{\sigma,x}$ and $\omega_{\Omega_i,x}$, respectively.

2.2.1 Explicit Time Integration Method

The spatial discretization leads to a semi-discrete system of ordinary differential equations in time

$$\frac{\partial q}{\partial t} + R(q) = 0. \tag{8}$$

The following explicit three-stage third order accurate Runge-Kutta time integration method is used to solve (8):

$$\begin{aligned} q^{(1)} &= q^n + \Delta t R(q^n, t^n) \\ q^{(2)} &= \frac{3}{4}q^n + \frac{1}{4}\Big(q^{(1)} + \Delta t R(q^{(1)}, t^n + \Delta t)\Big) \\ q^{n+1} &= \frac{1}{3}q^n + \frac{2}{3}\Big(q^{(2)} + \Delta t R(q^{(2)}, t^n + \frac{1}{2}\Delta t)\Big) \end{aligned} \tag{9}$$

Applied to the DG system with elements of order p this method has been shown to be linearly stable for a Courant number less than or equal to $\frac{1}{2p+1}$, cf. [4].

3 BOUNDARY TREATMENT

A detailed description of solid wall slip and Riemann boundary conditions is summarized in [2]. In this work these boundary conditions are imposed on the Gauss points of the interior and exterior boundary faces.

3.1 Curved Faces

In order to avoid oscillatory results near curved boundaries, a modified discretization independent of the choice of boundary condition is necessary. Therefore, for elements adjacent to curved solid walls the standard linear parametrization is replaced with a polynomial representation on a reference element $\hat{\Omega}$ of the order q

$$x = \sum_{k=1}^{n(q)} x_k \psi_k(\xi) \qquad \forall \xi \in \hat{\Omega}. \tag{10}$$

Here, the transformation from the reference element to the curved element is expressed in terms of Lagrange polynomials ψ_k and is calculated using additional points on the curved boundary.

The corresponding formulas for the surface and volume integration as well as the face normal vectors must be adapted. More precisely, the Jacobians of the higher-order geometric mapping are no longer constant and the integrals (6) and (7) have to be modified.

In this work, quadratic and cubic polynomials are used in (10). Therefore, the surface integral (6) is recalculated as follows

$$\sum_{\xi \in \mathcal{G}_{\hat{\sigma}}} \omega_{\hat{\sigma},\xi} \hat{\phi}_{i,k}(\xi) F_{\text{num}}^{\vec{n}_\sigma}(q_{h,i}(\xi), q_{h,j}(\xi)) \, \text{area}_\sigma(\xi) |\hat{\sigma}|,$$

here $\hat{\sigma}$ denotes the reference face. The curved face area for an integration point ξ is given by

$$\text{area}_\sigma(\xi) = \sqrt{\det \left[\left(\frac{\partial \psi(\xi)}{\partial \xi} \right)^T \left(\frac{\partial \psi(\xi)}{\partial \xi} \right) \right]}.$$

Moreover, the normal vectors $\vec{n}_\sigma$ have to be recalculated. For instance, if the face σ corresponds to $\{\xi = 0\}$ in the reference element, then we set

$$\vec{n}_\sigma = -\frac{\nabla \xi}{\|\nabla \xi\|}, \quad \nabla \xi = \left(\frac{\partial \xi}{\partial x}, \frac{\partial \xi}{\partial y}, \frac{\partial \xi}{\partial z} \right),$$

i.e., the normal vectors are calculated as linear combinations of the rows of the inverse Jacobian.

The volume integrals (7) are recalculated by

$$\sum_{\xi \in \mathcal{G}_{\hat{\Omega}}} \omega_{\hat{\Omega},\xi} F^{((J_i(\xi))^{-1} \nabla_\xi \hat{\phi}_{i,k}(\xi))}(q_{h,i}(\xi)) \, \det J_i(\xi) |\hat{\Omega}|,$$

where the Jacobian of the parametrization

$$J_i(\xi) = \sum_{k=1}^{n(q)} x_k \frac{\partial \psi_k(\xi)}{\partial \xi}$$

is used. Similarly, taking into account the non-constant Jacobians, the mass matrices are modified for the elements with curved faces.

4 PROCESS CHAIN FOR TURBOMACHINERY APPLICATIONS

In addition to the implementation of the DG scheme in the flow solver, the pre- and processing tools are generalized.

4.1 Preprocessing: Representation of Curved Boundaries

In order to provide geometric high-order information at curved solid walls an additional preprocessing step, in addition to the mesh generation, is necessary for the DG computations. For this purpose it is assumed that the user generates a fine auxiliary mesh which represents the curved surfaces to a very high accuracy.

At the first step, we perform a refinement of the boundary surface in accordance with the required order p. The additional intermediate nodes then allow the elements to be

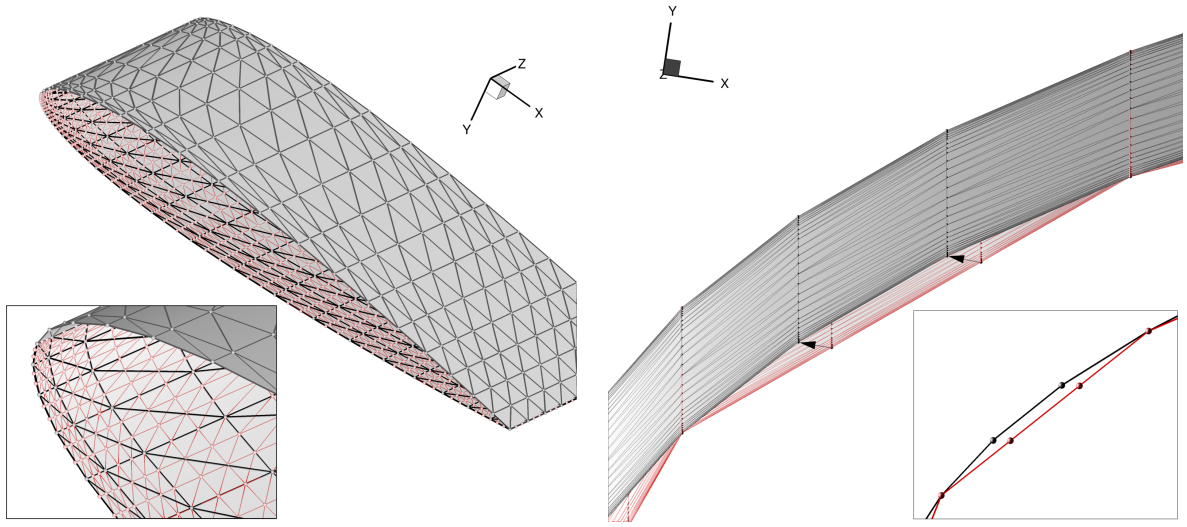

(a) (b)

Figure 1: Comparison of curved and straight surfaces of the blade profile.

replaced with two-dimensional high-order representations of the linear elements. In order to interpolate the coordinates of the fine auxiliary mesh to these higher order surfaces, the *mapping* functionality of DLR's preprocessor tool PREP is employed [10].

Originally the mapping task of PREP was developed in order to map blade eigenmodes, obtained from an FE tool for structure analysis, to surface displacements of the CFD mesh. The interpolation determines, for each point of the target mesh, the nearest face of the FE mesh. Then, using a second order accurate interpolation the displacement vectors are interpolated from the FE faces to the CFD mesh points. However, this task can be extended so that, instead of the surface displacements, the surface coordinates themselves are mapped from the FE geometry to the CFD mesh. For the application in the DG preprocess we apply this coordinate mapping to the fine auxiliary mesh and thus obtain a correction of the intermediate surface points of the higher order element representation of the curved boundary. For an illustration of this process see Fig. 1.

The higher order, curved boundary faces are stored in an additional two-dimensional zones in the CGNS file. During the initialization of the flow solver these additional zones are read and the intermediate nodes are used to obtain the higher order parametrization of the three-dimensional elements neighbouring the curved surface, cf. Eqn. (10).

4.2 Post-Processing: Interpolation on Refined Mesh

The post-processor POST developed for the CFD solver TRACE is highly modular, which allows the process chain to easily extended or modified, cf. [11]. The task concept of POST allows the developer to define a task sequence with possibilities to access complete data sets, modify meshes and flow solutions. Therefore, this software offers the integration

of new functionalities while keeping the benefits from the already existing tasks developed for post-processing.

Our approach for visualization and post processing of high-order DG solutions consists of the refinement of 3D elements into linear sub-elements, such as hexahedra, prisms, pyramids, or tetrahedra. Fig. 3 shows the comparison of the original coarse mesh and the refined mesh in 2D perspective.

Finally, the solutions $q_{h,i}(x,t)$ on these fine sub-mesh vertices are reconstructed from coefficients $q_{i,l}(t)$ using the polynomial basis $\phi_{i,l}(\xi_1,\xi_2,\xi_3)$ of order p on the coarse high-order element mesh. The workflow diagram of this process chain is shown in Fig. 2.

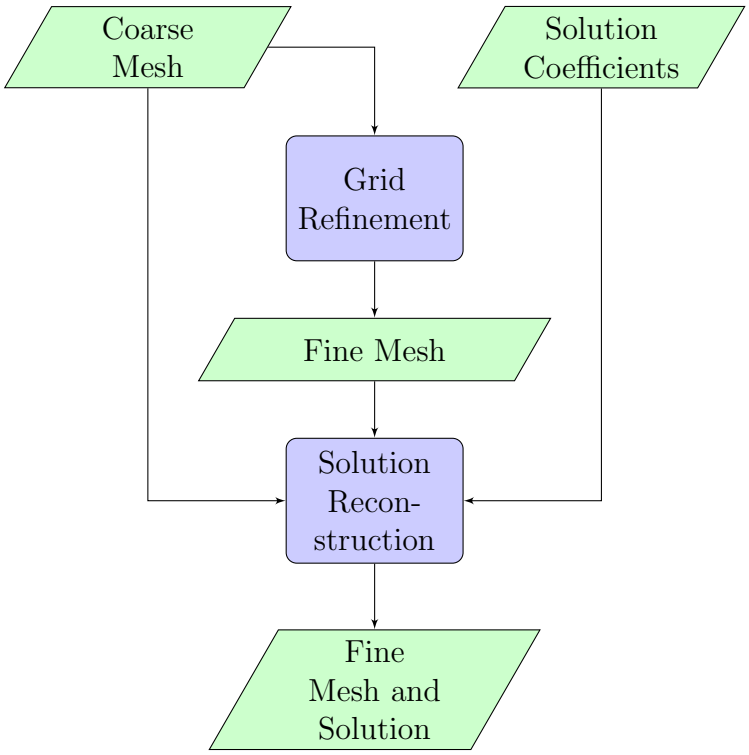

Figure 2: Workflow diagram of the post-processor tasks.

5 NUMERICAL EXAMPLE: NACA 0012

To demonstrate the functionalities developed in the DG solver and in the preprocessor for the treatment of curved boundaries, the simulation results for the flow around a NACA 0012 airfoil are presented.

The Mach number is set to $M_\infty = 0.3$ at zero angle of attack. All numerical simulations are done on the three-dimensional domain which is resolved 7026 tetrahedral elements as shown in Fig. 3(a). At the inlet and outlet boundaries Riemann boundary conditions are

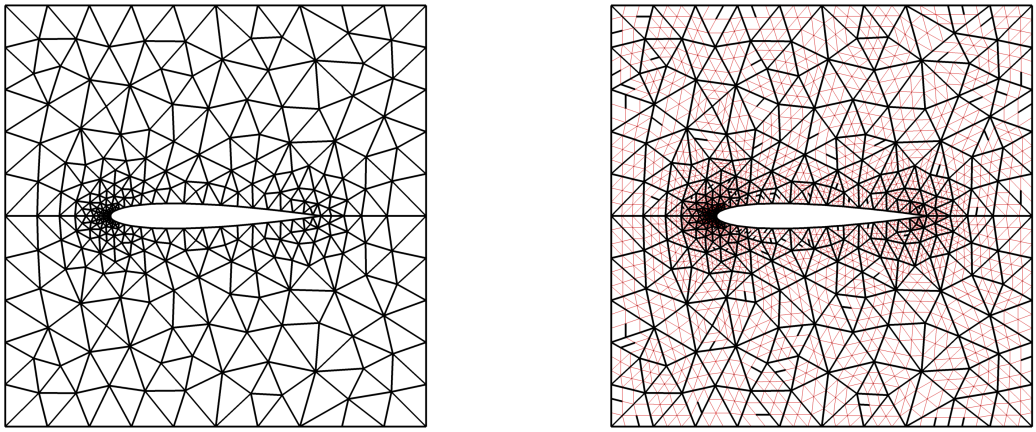

(a) Coarse initial mesh (b) Refined mesh (red)

Figure 3: Comparison of the original coarse mesh and the refined mesh.

imposed. The convergence criterion is satisfied when the root-mean-square error of the residual (based on the conservative variables) reaches a value of approximately 10^{-5}.

The pressure distributions for the solutions obtained with cubic elements are shown in Fig. 4. Whereas the steady solutions obtained on the straight boundary elements (Fig. 4(a)) show spurious disturbances, the simulation result obtained with a high-order geometrical representation of boundary elements (Fig. 4(b)) are of high quality.

6 CONCLUSIONS AND FUTURE WORK

This paper presents the integration of the DG method into the turbomachinery flow solver TRACE. The pre- and post-processing tools of the TRACE process chain have been extended. Since the new solver employs up to fourth order elements for the spatial discretization, the importance of an additional high order mesh at the curved boundaries has been demonstrated. Moreover, we have outlined the visualization strategy for high-order elements through the post-processing tool which provides the interpolation of the DG coefficients into the vertices of the refined mesh.

Future work will focus on the integration of viscous fluxes, the implementation of efficient implicit time-integration schemes as well as two-dimensional non-reflecting boundary conditions.

REFERENCES

[1] F. Bassi and S. Rebay. High-order accurate discontinuous solution of the 2D Euler equations. *Journal of computational physics*, 138:251–285, 1997.

[2] S. Cherednichenko, C. Frey, and G. Ashcroft. On the application of the discontinu-

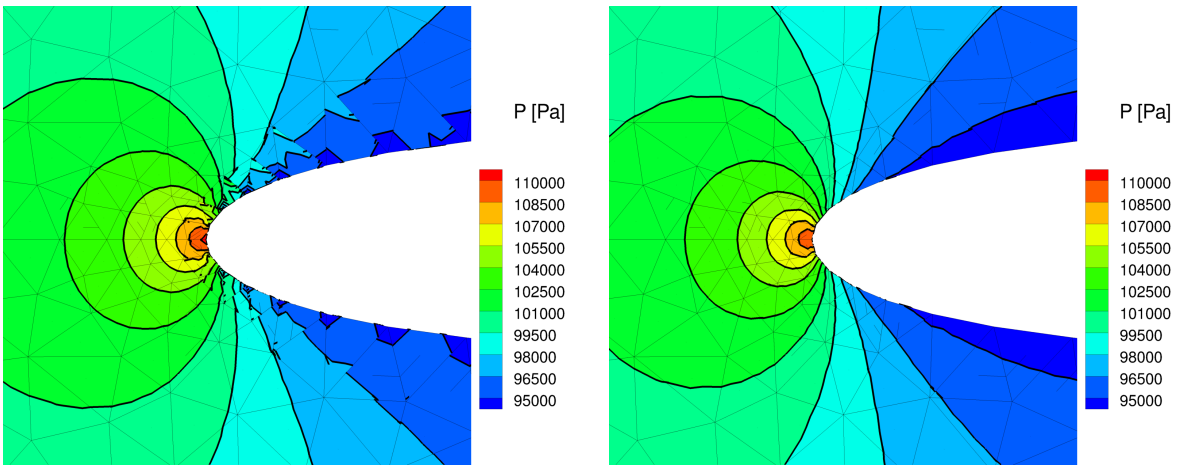

(a) Straight boundary elements (b) Curved boundary elements

Figure 4: Comparison of contour plots computed by DG solver with the polynomial order $p = 3$.

ous galerkin method to turbomachinery flows. In *6th European Congress on Computational Methods in Applied Sciences and Engineering (ECCOMAS 2012)*, pages 2359–2375, September 2012.

[3] B. Cockburn. *Discontinuous Galerkin methods for convection-dominated problems. High-order methods for computational physics, Lecture Notes in Computational Science and Engineering, 69–224.*, volume 9. Springer, 1999.

[4] B. Cockburn and C. Shu. Runge-Kutta discontinuous Galerkin methods for convection-dominated problems. *Journal of Scientific Computing*, 16(3):173–261, 2001.

[5] B. Cockburn and C.-W. Shu. TVD Runge-Kutta local projection discontinuous Galerkin finite element method for conservation laws ii: General framework. *Mathematics of Computations*, 52(186):411–435, 1989.

[6] B. Cockburn and C.-W. Shu. The Runge-Kutta discontinuous Galerkin method for conservation laws v: Multidimensional systems. *J. Computational Physics*, 141(1998):199–224, 1997.

[7] L. Krivodonova and M. Berger. High-order accurate implementation of solid wall boundary conditions in curved geometries. *J. Computational Physics*, (211):492–512, 2006.

[8] D. Mavriplis, N. C., K. Shahbazi, L. Wang, and N. Burgess. Progress high-order discontinuous Galerkin methods for aerospace applications. *AIAA Aerospace Sciences Meeting Including The New Horizons Forum and Aerospace Exposition*, 601, 2009.

[9] W. H. Reed and T. R. Hill. Triangular mesh methods for the neutron transport equation. Technical report, Los Alamos Scientific Laboratory, 1973.

[10] C. Voigt, C. Frey, and H.-P. Kersken. Development of a generic surface mapping algorithm for fluid-structure-interaction simulations in turbomachinery. In J. C. F. Pereira, A. Sequeira, and J. M. C. Pereira, editors, *V European Conference on Computational Fluid Dynamics ECCOMAS CFD 2010*, June 2010.

[11] C. Voigt, E. Kügeler, J. Wellner, and C. Morsbach. Conquer the terabyte scale: Post-processing of high resolution unsteady CFD data for turbomachinery analysis. In *6th European Congress on Computational Methods in Applied Sciences and Engineering (ECCOMAS 2012)*, September 2012.